Adaptive hp-finite element computations for time-harmonic Maxwell's equations

Xue Jiang[1], Linbo Zhang[1], and Weiying Zheng[1,*]

[1] *LSEC, Institute of Computational Mathematics, Academy of Mathematics and Systems Science, Chinese Academy of Sciences, Beijing, 100190, China.*

Abstract. In this paper, hp-adaptive finite element methods are studied for time-harmonic Maxwell's equations. We propose the parallel hp-adaptive algorithms on conforming unstructured tetrahedral meshes based on residual-based a posteriori error estimates. Extensive numerical experiments are reported to investigate the efficiency of the hp-adaptive methods for point singularities, edge singularities, and an engineering benchmark problem of Maxwell's equations. The hp-adaptive methods show much better performance than the h-adaptive method.

AMS subject classifications: 65M30, 78A45

Key words: hp-adaptive finite element method, Maxwell's equations, eddy current problem, a posteriori error estimate.

1 Introduction

Let $\Omega\subset\mathbb{R}^3$ be a bounded polygonal domain with Lipschitz continuous boundary $\Gamma=\partial\Omega$. Given a current density $\boldsymbol{f}$ with $\operatorname{div}\boldsymbol{f}=0$, we seek a solution $\boldsymbol{u}$ which satisfies the following time-harmonic Maxwell's equations (cf. e.g. [31, Chapter 1])

$$\mathbf{curl}(\mu_r^{-1}\mathbf{curl}\,\boldsymbol{u})-\kappa^2\alpha\boldsymbol{u}=\boldsymbol{f}\quad\text{in }\Omega, \tag{1.1a}$$

$$\mu_r^{-1}\mathbf{curl}\,\boldsymbol{u}\times\boldsymbol{n}=0\quad\text{on }\Gamma, \tag{1.1b}$$

where $\mu_r\geq 1$ is the relative magnetic permeability, $\kappa>0$ is the constant wave number, and α is the complex relative dielectric coefficient. Usually $\boldsymbol{u}$ stands for the electric field or the magnetic vector potential. In this paper, we are interested in two kinds of applications of (1.1). For $\alpha=\varepsilon_r-\mathbf{i}\sigma(\omega\varepsilon_0)^{-1}$, (1.1) describes the electromagnetic field at moderate or high frequencies. For $\alpha=-\mathbf{i}\sigma(\omega\varepsilon_0)^{-1}$, (1.1) is the eddy current model which approximates the Maxwell equations at very low frequency [3]. Here $\varepsilon_r\geq 1$ is the physical relative

*Corresponding author. *Email addresses:* jxue@lsec.cc.ac.cn (X. Jiang), zlb@lsec.cc.ac.cn (L. Zhang), zwy@lsec.cc.ac.cn (W. Zheng)

dielectric coefficient, $\varepsilon_0 > 0$ is the dielectric coefficient in the empty space, $\sigma \geq 0$ is the the electric conductivity, and $\omega > 0$ is the constant angular frequency. For the eddy current model, we assume that Γ is the truncated boundary of $\mathbb{R}^3$ and Ω is *simply connected*. The homogeneity of the boundary condition in (1.1b) is not essential for our analysis but simplifies our proofs.

In this paper, we study the hp-adaptive finite element method for (1.1) on tetrahedral meshes. Since the pioneering work of Babuška and Rheinboldt [8], the self-adaptive finite element method based on a posteriori error estimates has been studied over thirty years. It has become one of the most popular methods in the numerical solution of partial differential equations and in scientific and engineering computing. As for the h-adaptive method which reduces the error by local mesh refinements, great successes have been achieved in the study of a posteriori error analysis (cf. e.g. [11, 16, 38]), mesh refinement algorithms (cf. e.g. [4, 25, 39]), and convergence and optimal complexity (cf. e.g. [21, 24, 32]). Recently, Schöberl and coauthors studied h-type a posteriori error estimates for Maxwell's equations. In [14], Braess and Schöberl proposed the equilibrated residual error estimator for edge elements with unit reliability constant. In [37], Schöberl proved the reliability of the residual-based a posteriori error estimate for Maxwell's equations via commuting quasi-interpolation operators. Using the idea of error equidistribution, the h-adaptive method based on a posteriori error estimates could yield a quasi-optimal approximation with algebraic convergence rate

$$\eta_h \approx C N_h^{-p/d}, \tag{1.2}$$

where η_h is the a posteriori error estimate, d is the spatial dimension, p is the order of the finite element method, and N_h is the number of degrees of freedom. However, due to the singularity of the solution, the quasi-optimality (1.2) will degenerate for higher-order finite elements since the constant C may blow up with increasing p.

The hp-adaptive finite element method reduces the error by both local mesh refinements and local increase of polynomial degrees. It is more efficient than the pure h-adaptive and p-adaptive methods and could reduce the error exponentially. For example, the optimal convergence rate of the hp-adaptive method is

$$\eta_{hp} \approx C e^{-\delta N_{hp}^{1/3}} \tag{1.3}$$

for two dimensional elliptic problems [22], and is also conjectured to be

$$\eta_{hp} \approx C e^{-\delta N_{hp}^{1/5}} \tag{1.4}$$

for three dimensional elliptic problems [6], where C, δ are positive constants independent of h and p, η_{hp} is the a posteriori error estimate for the hp-adaptive method, and N_{hp} is the number of degrees of freedom. But for solutions with edge singularities, the meshes leading to the convergence rate in (1.4) must be obtained by anisotropic refinements, that is, by using "needle elements" which are parallel to the edges (see [6] for more comments).

Theoretical studies on *hp*-adaptive methods arose in the early 1980s (cf. [7, 9]) and now has attracted more and more attentions.

The implementation of the *hp*-adaptive method is very challenging for higher dimensional problems. Thus most of the works in 1980s focused on theoretical aspects. From 1990s on, more attention has been paid to the study of *hp*-adaptive algorithms and practical implementations. And most of the literature focused on the *hp*-adaptive computations of two-dimensional problems (cf. e.g. [2, 23, 27–29, 34]). Recently, using goal-oriented a posteriori error estimates, Demkowicz and coauthors carried out *hp*-adaptive simulations of resistivity logging-while-drilling measurements on hexahedral meshes [19, 35]. Based on unstructured tetrahedral meshes and MPI, Zhang and Liu implemented a parallel *hp*-adaptive finite element method for elliptic problems [26, 39].

In this paper, we first derive an *hp*-type a posteriori error estimate for the time-harmonic Maxwell's equations. The a posteriori error estimate is residual-based and reliable with the generic constant C independent of h and p. We also refer to [13, 17, 27, 28] for *hp*-type a posteriori error estimates for elliptical problems. Next we propose two *hp*-adaptive algorithms for solving (1.1). The first algorithm is an extension of the *hp*-adaptive algorithm in [26, Section 5.3.1] to Maxwell's equations and uses the strategy of predicted error reductions. The second algorithm is proposed upon using the maximum strategy. We implemented parallel *hp*-adaptive edge element methods on unstructured tetrahedral meshes. We present five numerical experiments to study the efficiency of the *hp*-adaptive algorithms. The first experiment is the Fichera problem which has a point singularity at the reentrant corner of the domain. The *hp*-adaptive methods show exponential decay of the a posteriori error estimate and the approximation error

$$\eta_{hp} \approx Ce^{-\gamma N_{hp}^{1/5}}, \qquad \|\boldsymbol{u}-\boldsymbol{u}_h\|_{\boldsymbol{H}(\mathbf{curl},\Omega)} \approx Ce^{-\gamma N_{hp}^{1/5}}, \qquad \gamma = 0.95.$$

The second experiment investigates the performance of the *hp*-adaptive methods for single edge singularity. The third experiment compares the *hp*-adaptive method based on a posteriori error estimates and the a priori *hp*-adaptive method based on anisotropic refinements along the edge of singularity. The anisotropic *hp*-adaptive algorithm yields exponential decay of the error. The isotropic *hp*-adaptive method performs worse than the *hp*-adaptive method using anisotropic refinements, but much better than the *h*-adaptive method. The fourth experiment investigates the performance of the *hp*-adaptive methods for multiple edge singularities. The last experiment solves an engineering benchmark — Team Workshop Problem 21-a2. For this example, the *hp*-adaptive methods show much better performance than the *h*-adaptive method.

The rest of the paper is arranged as follows: In Section 2, we present a weak formulation of (1.1) and establish the wellposedness of the problem. In Section 3, we introduce the *hp*-edge element approximation to (1.1) and derive the *hp*-type a posteriori error estimates. In Section 4, we propose two *hp*-adaptive algorithms based on the a posteriori error estimate. In Section 5, we report five numerical experiments to demonstrate the competitive behavior of the *hp*-adaptive methods.

2 Weak formulation

We start by introducing some notation and Sobolev spaces used in this paper. Let $L^2(\Omega)$ be the usual Hilbert space of square integrable functions equipped with the following inner product and norm:

$$(u,v) := \int_\Omega u(\boldsymbol{x})\bar{v}(\boldsymbol{x})\mathrm{d}\boldsymbol{x} \quad \text{and} \quad \|u\|_{L^2(\Omega)} := (u,v)^{1/2},$$

where $\bar{v}$ is the complex conjugate of v. Let $H^m(\Omega) := \{v \in L^2(\Omega) : D^\xi v \in L^2(\Omega), |\xi| \le m\}$ be equipped with the following norm and semi-norm

$$\|u\|_{H^m(\Omega)} := \Big(\sum_{|\xi|\le m} \left\| D^\xi u \right\|^2_{L^2(\Omega)} \Big)^{1/2} \quad \text{and} \quad |u|_{H^m(\Omega)} := \Big(\sum_{|\xi|= m} \left\| D^\xi u \right\|^2_{L^2(\Omega)} \Big)^{1/2},$$

where ξ represents non-negative triple index. Let $H^1_0(\Omega)$ be the subspace of $H^1(\Omega)$ whose functions have zero traces on Γ. Throughout the paper we denote vector-valued quantities by boldface notation, such as $\boldsymbol{L}^2(\Omega) := (L^2(\Omega))^3$. Define

$$\begin{aligned} \boldsymbol{H}(\mathbf{curl},\Omega) &:= \big\{ \boldsymbol{v} \in \boldsymbol{L}^2(\Omega) : \mathbf{curl}\, \boldsymbol{v} \in \boldsymbol{L}^2(\Omega) \big\}, \\ \boldsymbol{H}_0(\mathbf{curl},\Omega) &:= \big\{ \boldsymbol{v} \in \boldsymbol{H}(\mathbf{curl},\Omega) : \boldsymbol{v} \times \boldsymbol{n} = 0 \text{ on } \Gamma \big\}, \end{aligned}$$

which are equipped with the following norm:

$$\|\boldsymbol{v}\|_{\boldsymbol{H}(\mathbf{curl},\Omega)} := \Big(\|\boldsymbol{v}\|^2_{L^2(\Omega)} + \|\mathbf{curl}\, \boldsymbol{v}\|^2_{L^2(\Omega)} \Big)^{1/2}.$$

We denote the conducting domain by $\Omega_c \subset \Omega$ and the insulating domain by $\Omega_i = \Omega \backslash \overline{\Omega}_c$. For the eddy current model, we denote $\Sigma = \partial\Omega_c$ and assume that $\overline{\Omega}_c \subset \Omega$ and $\Gamma \cap \Sigma = \emptyset$. Furthermore, we make the following assumptions on the parameters which are mild in physical settings:

(H1) $\kappa > 0$ is constant and μ, α are piecewise constant in Ω.

(H2) There are constants $\mu_{\min}, \mu_{\max}$ such that $0 < \mu_{\min} \le \mu \le \mu_{\max}$ in Ω.

(H3) There are constants $0 < \alpha_{\min} \le \alpha_{\max}$ such that

$$\begin{aligned} &\alpha_{\min} \le \mathrm{Re}\alpha \le \alpha_{\max} \quad \text{in } \Omega \qquad \text{or} \qquad \mathrm{Re}\alpha \equiv 0 \quad \text{in } \Omega, \\ &\alpha_{\min} \le \mathrm{Im}\alpha \le \alpha_{\max} \quad \text{in } \Omega_c \qquad \text{and} \qquad \mathrm{Im}\alpha \equiv 0 \quad \text{in } \Omega_i. \end{aligned}$$

To distinguish the two model problems, we shall use $\alpha|_{\Omega_i} \neq 0$ for the model at moderate or high frequencies and use $\alpha|_{\Omega_i} = 0$ for the eddy current model in the rest of the paper.

Now we present a weak formulation of (1.1): Find $\boldsymbol{u} \in \boldsymbol{H}(\mathbf{curl},\Omega)$ such that

$$a(\boldsymbol{u},\boldsymbol{v}) = (\boldsymbol{f},\boldsymbol{v}) \qquad \forall \boldsymbol{v} \in \boldsymbol{H}(\mathbf{curl},\Omega), \tag{2.1}$$

where the sesquilinear form a: $\boldsymbol{H}(\mathbf{curl},\Omega)\times\boldsymbol{H}(\mathbf{curl},\Omega)\to\mathbb{C}$ is defined by

$$a(\boldsymbol{u},\boldsymbol{v}):=\int_\Omega(\mu^{-1}\mathbf{curl}\,\boldsymbol{u}\cdot\mathbf{curl}\,\bar{\boldsymbol{v}}-\kappa^2\alpha\boldsymbol{u}\cdot\bar{\boldsymbol{v}}). \tag{2.2}$$

For $\alpha|_{\Omega_i}\neq 0$, the existence and uniqueness of the solution $\boldsymbol{u}\in\boldsymbol{H}(\mathbf{curl},\Omega)$ have been established in [31, Chapter 4]. If $\mathrm{Im}\alpha=0$, the differential operator in (1.1) could have resonant modes, and thus problem (1.1) could be ill-posed for some $\boldsymbol{f}$. We do not elaborate on this case here.

For $\alpha|_{\Omega_i}=0$, we introduce a subspace

$$\boldsymbol{X}=\left\{\boldsymbol{v}\in\boldsymbol{H}(\mathbf{curl},\Omega):(\boldsymbol{v},\nabla p)=0\;\forall p\in H_c^1(\Omega)\right\},$$

where $H_c^1(\Omega)=\left\{p\in H^1(\Omega):p=\text{Const. in }\overline{\Omega}_c\right\}$. Define

$$(\boldsymbol{u},\boldsymbol{v})_{\boldsymbol{X}}=\int_{\Omega_c}\boldsymbol{u}\cdot\bar{\boldsymbol{v}}+\int_\Omega\mathbf{curl}\,\boldsymbol{u}\cdot\mathbf{curl}\,\bar{\boldsymbol{v}}\qquad\text{and}\qquad\|\boldsymbol{v}\|_{\boldsymbol{X}}=\sqrt{(\boldsymbol{v},\boldsymbol{v})_{\boldsymbol{X}}}. \tag{2.3}$$

From (H3) and (2.2)–(2.3) we deduce that

$$|a(\boldsymbol{v},\boldsymbol{v})|\geq\min(\mu_{\max}^{-1},\alpha_{\min})\,\|\boldsymbol{v}\|_{\boldsymbol{X}}^2\qquad\forall\boldsymbol{v}\in\boldsymbol{X}. \tag{2.4}$$

It is known that $\|\cdot\|_{\boldsymbol{X}}$ and $\|\cdot\|_{\boldsymbol{H}(\mathbf{curl},\Omega)}$ are equivalent norms on $\boldsymbol{X}$ (cf. [10,15] for the case that $\boldsymbol{X}\subset\boldsymbol{H}_0(\mathbf{curl},\Omega)$). Then (2.1) has a unique solution $\boldsymbol{u}\in\boldsymbol{X}$.

For $\alpha|_{\Omega_i}\neq 0$, the existence and uniqueness of (2.1) indicates the following inf-sup condition (cf. e.g. [5, Chapter 5])

$$\sup_{0\neq v\in\boldsymbol{H}(\mathbf{curl},\Omega)}\frac{|a(\boldsymbol{w},\boldsymbol{v})|}{\|\boldsymbol{v}\|_{\boldsymbol{H}(\mathbf{curl},\Omega)}}\geq\beta\|\boldsymbol{w}\|_{\boldsymbol{H}(\mathbf{curl},\Omega)}\quad\forall\boldsymbol{w}\in\boldsymbol{H}(\mathbf{curl},\Omega), \tag{2.5}$$

where $\beta>0$ is a constant only depending on μ, κ, α, and Ω. For $\alpha|_{\Omega_i}=0$, using (2.4) and the norm equivalence on $\boldsymbol{X}$ and setting β small enough, we also have

$$\sup_{0\neq\boldsymbol{v}\in\boldsymbol{X}}\frac{|a(\boldsymbol{w},\boldsymbol{v})|}{\|\boldsymbol{v}\|_{\boldsymbol{H}(\mathbf{curl},\Omega)}}\geq\beta\|\boldsymbol{w}\|_{\boldsymbol{H}(\mathbf{curl},\Omega)}\qquad\forall\boldsymbol{w}\in\boldsymbol{X}. \tag{2.6}$$

Furthermore, (2.5)–(2.6) indicate that the following stability estimate holds :

$$\|\boldsymbol{u}\|_{\boldsymbol{H}(\mathbf{curl},\Omega)}\leq C\|\boldsymbol{f}\|_{0,\Omega}. \tag{2.7}$$

3 Finite element approximations

Let $\mathcal{T}_h$ be a shape-regular tetrahedral triangulation of Ω in the sense that

$$\max_{K\in\mathcal{T}_h}(h_K/\rho_K)\leq C, \tag{3.1}$$

where $C>0$ is a constant independent of $\mathcal{T}_h$, h_K is the diameter of K, and ρ_K is the diameter of the inscribed ball of K. We assume that $\mathcal{T}_h$ is conforming such that the intersection $\overline{K}_1\cap\overline{K}_2$ of any two elements $K_1,K_2\in\mathcal{T}_h$ is empty, or a vertex, or an edge, or a whole face. We denote the set of faces, the set of edges, and the set of vertices of D by $\mathcal{F}(D)$, $\mathcal{E}(D)$, $\mathcal{V}(D)$ respectively, where D may stand for $\mathcal{T}_h$, or an element K, or a face F, or an edge E in different settings.

3.1 The discrete problem

We endow each $K\in\mathcal{T}_h$ with a polynomial degree $p_K\in\mathbb{N}$ and collect the polynomial degrees by $\mathcal{P}_h:=\{p_K:\forall K\in\mathcal{T}_h\}$. We assume that $\mathcal{P}_h$ satisfies

$$|p_K-p_{K'}|\le\gamma\qquad\forall K,K'\in\mathcal{T}_h \text{ satisfying } \overline{K}\cap\overline{K'}\neq\emptyset, \tag{3.2}$$

where γ is a constant independent of $\mathcal{T}_h$. For any $\mathbf{v}\in\mathcal{V}(\mathcal{T}_h)$, $E\in\mathcal{E}(\mathcal{T}_h)$, and $F\in\mathcal{F}(\mathcal{T}_h)$, we also employ the minimum rule [27] to define the the degrees of $\mathbf{v}$, E, and F :

$$p_{\mathbf{v}}=\min\{p_K:\mathbf{v}\in\mathcal{V}(K)\},\quad p_E=\min\{p_K:E\in\mathcal{E}(K)\},\quad p_F=\min\{p_K:F\in\mathcal{F}(K)\}. \tag{3.3}$$

Clearly the definitions in (3.3) are associated with $\mathcal{P}_h$ and should be denoted by $p_{\mathbf{v}}(\mathcal{P}_h)$, $p_E(\mathcal{P}_h)$, $p_F(\mathcal{P}_h)$ for any $\mathbf{v}$, E, and F. Without confusion in specific circumstance, we omit the dependence on $\mathcal{P}_h$ to simplify the notation. Using the minimum rule, the finite element spaces of variable order are defined as follows

$$\begin{aligned} V(\mathcal{T}_h,\mathcal{P}_h) &= \Big\{v\in H^1(\Omega):v|_K\in P_{p_K}(K)\quad\forall K\in\mathcal{T}_h\Big\},\\ \boldsymbol{U}(\mathcal{T}_h,\mathcal{P}_h) &= \Big\{\boldsymbol{v}\in\boldsymbol{H}(\mathbf{curl},\Omega):\boldsymbol{v}|_K\in\big(P_{p_K}(K)\big)^3\quad\forall K\in\mathcal{T}_h\Big\}, \end{aligned}$$

where $P_m(K)=\mathrm{Span}\Big\{x_1^ix_2^jx_3^k:0\le i+j+k\le m,(x_1,x_2,x_3)\in K\Big\}$ for any integer $m\ge0$.

We also define the finite element spaces of fixed orders

$$\begin{aligned} V(\mathcal{T}_h,m) &= \Big\{v\in H^1(\Omega):v|_K\in P_m(K)\quad\forall K\in\mathcal{T}_h\Big\},\\ \boldsymbol{U}(\mathcal{T}_h,m) &= \Big\{\boldsymbol{v}\in\boldsymbol{H}(\mathbf{curl},\Omega):\boldsymbol{v}|_K\in\big(P_m(K)\big)^3\quad\forall K\in\mathcal{T}_h\Big\}. \end{aligned}$$

The definitions are associated with the uniform distribution $\{p_K=m:\forall K\in\mathcal{T}_h\}$ and also reflect the minimum rule

$$p_{\mathbf{v}}=p_E=p_F=m\qquad\forall\mathbf{v}\in\mathcal{V}(\mathcal{T}_h),E\in\mathcal{E}(\mathcal{T}_h),F\in\mathcal{F}(\mathcal{T}_h).$$

The Galerkin approximation to (2.1) reads: Find $\boldsymbol{u}_{hp}\in\boldsymbol{U}(\mathcal{T}_h,\mathcal{P}_h)$ such that

$$a(\boldsymbol{u}_{hp},\boldsymbol{v})=(\boldsymbol{f},\boldsymbol{v})\qquad\forall\boldsymbol{v}_h\in\boldsymbol{U}(\mathcal{T}_h,\mathcal{P}_h). \tag{3.4}$$

For $\alpha|_{\Omega_i}\neq0$, the existence and uniqueness of $\boldsymbol{u}_{hp}\in\boldsymbol{U}(\mathcal{T}_h,\mathcal{P}_h)$ can be proved by similar arguments as in [31, Chapter 7]. We do not elaborate on the details here. For $\alpha|_{\Omega_i}=0$, the well-posedness of (3.4) is given by the following lemma.

Lemma 3.1. *Suppose* $\alpha=-\mathbf{i}\sigma(\omega\varepsilon_0)^{-1}$. *Then* (3.4) *has a unique solution*

$$\boldsymbol{u}_{hp}\in\boldsymbol{X}_{hp}=\big\{\boldsymbol{v}\in\boldsymbol{U}(\mathcal{T}_h,\mathcal{P}_h):(\boldsymbol{v},\nabla\varphi)=0\ \forall\varphi\in V_c(\mathcal{T}_h,\mathcal{P}_h+1)\big\},\tag{3.5}$$

where $V_c(\mathcal{T}_h,\mathcal{P}_h+1)=\big\{\varphi\in H_c^1(\Omega):\varphi|_K\in P_{p_K+1}(K)\quad\forall K\in\mathcal{T}_h\big\}$.

Proof. In view of the definition of $a(\cdot,\cdot)$, we need only prove that $\|\cdot\|_{\boldsymbol{X}}$ is a norm on $\boldsymbol{X}_{hp}$. Let $\boldsymbol{v}\in\boldsymbol{X}_{hp}$ satisfy $\|\boldsymbol{v}\|_{\boldsymbol{X}}=0$. Then we know that

$$\boldsymbol{v}=0\quad\text{in }\Omega_c\qquad\text{and}\qquad\mathbf{curl}\,\boldsymbol{v}=0\quad\text{in }\Omega.$$

Since Ω is simply connected, there exists a $\psi\in H_c^1(\Omega)/\mathbb{R}$ such that $\boldsymbol{v}=\nabla\psi$. But $\boldsymbol{v}$ is piecewise polynomial, hence $\psi\in V_c(\mathcal{T}_h,\mathcal{P}_h+1)$. The definition of $\boldsymbol{X}_{hp}$ indicates that $\|\nabla\psi\|_{L^2(\Omega)}=0$. This yields $\boldsymbol{v}=\nabla\psi=0$ in Ω. The proof is completed. □

3.2 A posteriori error estimates

The hp-type interpolation operator plays an important role in a posterior error estimates. In [27], Melenk constructed two-dimensional hp-interpolation operators onto the $H^1(\Omega)$-conforming finite element space. Here we present an hp-interpolation operator in three dimension. The proofs are similar to those in [27] and we do not elaborate on the details.

Theorem 3.1. *Let* $\mathcal{T}_h$ *be a shape-regular mesh and let* $\mathcal{P}_h$ *be a polynomial degree distribution on* $\mathcal{T}_h$ *satisfying* (3.2). *Then there exists a constant* $C>0$ *such that*

$$\big\|u-\Pi_{hp}u\big\|_{L^2(K)}+\frac{h_K}{p_K}\big\|\nabla(u-\Pi_{hp}u)\big\|_{L^2(K)}\le C\frac{h_K}{p_K}\|\nabla u\|_{L^2(\Omega_K)}\qquad\forall K\in\mathcal{T}_h,$$
$$\big\|u-\Pi_{hp}u\big\|_{L^2(F)}\le C\Big(\frac{h_F}{p_F}\Big)^{1/2}\|\nabla u\|_{L^2(\Omega_F)}\qquad\forall F\in\mathcal{F}(\mathcal{T}_h),$$

where

$$\Omega_K=\Big(\bigcup\{\overline{K'}:K'\in\mathcal{T}_h,\overline{K}\cap\overline{K'}\neq\emptyset\}\Big)^\circ,\quad\Omega_F=\Big(\bigcup\{\overline{K'}:K'\in\mathcal{T}_h,\overline{F}\cap\overline{K'}\neq\emptyset\}\Big)^\circ.$$

Now we derive the a posteriori error estimates for hp-adaptive finite element method. Let $\boldsymbol{u}$ and $\boldsymbol{u}_{hp}$ be the solutions of (2.1) and (3.4) respectively. Define the error function by $\boldsymbol{e}_{hp}=\boldsymbol{u}-\boldsymbol{u}_{hp}$. For $\alpha|_{\Omega_i}\neq0$, from (2.5) we know that

$$\big\|\boldsymbol{e}_{hp}\big\|_{\boldsymbol{H}(\mathbf{curl},\Omega)}\le\beta^{-1}\sup_{v\in\boldsymbol{H}_0(\mathbf{curl},\Omega)}\frac{\big|a(\boldsymbol{e}_{hp},\boldsymbol{v})\big|}{\|\boldsymbol{v}\|_{\boldsymbol{H}(\mathbf{curl},\Omega)}}.\tag{3.6}$$

For $\alpha|_{\Omega_i}=0$, we let $\boldsymbol{u}_{hp}\in\boldsymbol{X}_{hp}$ be the unique solution. Notice that $\boldsymbol{u}_{hp}\notin\boldsymbol{X}$, we let $\psi^{hp}\in H_c^1(\Omega)/\mathbb{R}$ be the unique solution of the variational problem:

$$(\nabla\psi^{hp},\nabla\varphi)=(\boldsymbol{u}_{hp},\nabla\varphi)\qquad\forall\varphi\in H_c^1(\Omega)/\mathbb{R}.\tag{3.7}$$

Then $\boldsymbol{u}^{hp}=\boldsymbol{u}_{hp}-\nabla\psi^{hp}\in\boldsymbol{X}$. From (2.6) we know that

$$\left\|\boldsymbol{u}-\boldsymbol{u}^{hp}\right\|_{\boldsymbol{H}(\mathbf{curl},\Omega)}\leq\beta^{-1}\sup_{v\in\boldsymbol{X}}\frac{\left|a(\boldsymbol{u}-\boldsymbol{u}^{hp},\boldsymbol{v})\right|}{\|\boldsymbol{v}\|_{\boldsymbol{H}(\mathbf{curl},\Omega)}}=\beta^{-1}\sup_{v\in\boldsymbol{X}}\frac{\left|a(\boldsymbol{e}_{hp},\boldsymbol{v})\right|}{\|\boldsymbol{v}\|_{\boldsymbol{H}(\mathbf{curl},\Omega)}}\leq\beta^{-1}\sup_{v\in\boldsymbol{H}(\mathbf{curl},\Omega)}\frac{\left|a(\boldsymbol{e}_{hp},\boldsymbol{v})\right|}{\|\boldsymbol{v}\|_{\boldsymbol{H}(\mathbf{curl},\Omega)}}.$$

It follows that

$$\left\|\boldsymbol{e}_{hp}\right\|_{\boldsymbol{X}}=\left\|\boldsymbol{u}-\boldsymbol{u}^{hp}\right\|_{\boldsymbol{X}}\leq\beta^{-1}\sup_{v\in\boldsymbol{H}(\mathbf{curl},\Omega)}\frac{\left|a(\boldsymbol{e}_{hp},\boldsymbol{v})\right|}{\|\boldsymbol{v}\|_{\boldsymbol{H}(\mathbf{curl},\Omega)}}.\tag{3.8}$$

For any face $F\in\mathcal{F}(\mathcal{T}_h)$, assuming $F=\partial K_1\cap\partial K_2$ with $K_1,K_2\in\mathcal{T}_h$, we denote the jump of a function v across F by $[v]_F:=v|_{K_1}-v|_{K_2}$. For convenience in notation, we define the residual functions on each $K\in\mathcal{T}_h$ and $F\in\mathcal{F}(\mathcal{T}_h)$ as follows

$$R_K=\operatorname{div}(\boldsymbol{f}+\kappa^2\alpha\boldsymbol{u}_{hp}|_K),\qquad \boldsymbol{R}_K=\boldsymbol{f}+\kappa^2\alpha\boldsymbol{u}_{hp}-\mathbf{curl}(\mu_r^{-1}\mathbf{curl}\,\boldsymbol{u}_{hp}|_K),\tag{3.9}$$

$$J_F=[(\boldsymbol{f}+\kappa^2\alpha\boldsymbol{u}_{hp})\cdot\boldsymbol{n}]_F,\qquad \boldsymbol{J}_F=[\mu_r^{-1}\mathbf{curl}\,\boldsymbol{u}_{hp}\times\boldsymbol{n}]_F.\tag{3.10}$$

Hereafter we extend $\boldsymbol{u}_{hp}$, $\boldsymbol{f}$ by zero to the exterior of Ω.

Theorem 3.2. *Let (H1)–(H3) be satisfied. There exists a constant C only depending on the inf-sup constant β in* (2.5)–(2.6) *and the local quasi-uniformity of $(\mathcal{T}_h,\mathcal{P}_h)$ such that*

$$\left\|\boldsymbol{e}_{hp}\right\|_{\boldsymbol{H}(\mathbf{curl},\Omega)}\leq C\eta_{hp}\quad \text{if } \alpha|_{\Omega_i}\neq 0\qquad \text{and}\qquad \left\|\boldsymbol{e}_{hp}\right\|_{\boldsymbol{X}}\leq C\eta_{hp}\quad \text{if } \alpha|_{\Omega_i}=0,\tag{3.11}$$

where η_{hp} is the a posteriori error estimate defined by

$$\eta_{hp}^2=\sum_{K\in\mathcal{T}_h}\Big(\frac{h_K}{p_K}\Big)^2\big\{\|R_K\|_{L^2(K)}^2+\|\boldsymbol{R}_K\|_{L^2(K)}^2\big\}+\sum_{F\in\mathcal{F}(\mathcal{T}_h)}\frac{h_F}{p_F}\big\{\|J_F\|_{L^2(F)}^2+\|\boldsymbol{J}_F\|_{L^2(F)}^2\big\}.\tag{3.12}$$

Proof. For any $\boldsymbol{v}\in\boldsymbol{H}(\mathbf{curl},\Omega)$, by the Birman-Solomyak decomposition [12,20], there exist $\varphi\in H^1(\Omega)$, $\boldsymbol{v}_s\in\boldsymbol{H}^1(\Omega)$ such that

$$\boldsymbol{v}=\nabla\varphi+\boldsymbol{v}_s,\qquad \|\varphi\|_{H^1(\Omega)}+\|\boldsymbol{v}_s\|_{H^1(\Omega)}\leq C\|\boldsymbol{v}\|_{\boldsymbol{H}(\mathbf{curl},\Omega)}.\tag{3.13}$$

Since $\nabla\Pi_{hp}\varphi+\Pi_{hp}\boldsymbol{v}_s\in\boldsymbol{U}(\mathcal{T}_h,\mathcal{P}_h)$, by the Galerkin orthogonality, we have

$$a(\boldsymbol{e}_{hp},\boldsymbol{v})=a(\boldsymbol{e}_{hp},\nabla\varphi-\nabla\Pi_{hp}\varphi)+a(\boldsymbol{e}_{hp},\boldsymbol{v}_s-\Pi_{hp}\boldsymbol{v}_s).\tag{3.14}$$

By similar arguments as in [11,16] and using Lemma 3.1, we deduce that

$$\begin{aligned}\left|a(\boldsymbol{e}_{hp},\nabla\varphi-\nabla\Pi_{hp}\varphi)\right| &\leq C\Big\{\sum_{K\in\mathcal{T}_h}\Big(\frac{h_K}{p_K}\Big)^2\|R_K\|_{L^2(K)}^2+\sum_{F\in\mathcal{F}(\mathcal{T}_h)}\frac{h_F}{p_F}\|J_F\|_{L^2(F)}^2\Big\}^{1/2}\|\varphi\|_{H^1(\Omega)},\\ \left|a(\boldsymbol{e}_{hp},\boldsymbol{v}_s-\Pi_{hp}\boldsymbol{v}_s)\right| &\leq C\Big\{\sum_{K\in\mathcal{T}_h}\Big(\frac{h_K}{p_K}\Big)^2\|\boldsymbol{R}_K\|_{L^2(K)}^2+\sum_{F\in\mathcal{F}(\mathcal{T}_h)}\frac{h_F}{p_F}\|\boldsymbol{J}_F\|_{L^2(F)}^2\Big\}^{1/2}\|\boldsymbol{v}_s\|_{H^1(\Omega)}.\end{aligned}$$

The proof is completed upon using (3.13)–(3.14) and the inf-sup conditions (3.6) and (3.8). □

Remark 3.1. Using similar arguments as in [11], we can prove the lower bound estimate

$$\eta_{hp} \le C \|\boldsymbol{e}_{hp}\|_{\boldsymbol{H}(\mathbf{curl},\Omega)} + C \sum_{K\in\mathcal{T}_h} h_K^2 \|f - Q_K f\|^2_{L^2(K)},$$

where Q_K: $L^2(K) \to P_{p_K}(K)$ is the L^2–projection operator. But the generic constant C will depend on the polynomial degree distribution $\mathcal{P}_h$ here. We also refer to [27,28] for similar discussions.

4 Hp–adaptive finite element algorithms

Let $\mathcal{T}_0 \prec \mathcal{T}_1 \prec \cdots \prec \mathcal{T}_L$ be a sequence of adaptively refined meshes and let $\mathcal{P}_l$ be the polynomial degree distribution over $\mathcal{T}_l$. For any element $K \in \mathcal{T}_l$, we define the local a posteriori error estimator η_K by

$$\eta_K = \frac{h_K}{p_K}\big(\|\boldsymbol{R}_K\|_{L^2(K)} + \|R_K\|_{L^2(K)}\big) + \frac{1}{2}\sum_{F\in\mathcal{F}(K)}\Big(\frac{h_F}{p_F}\Big)^{1/2}\big(\|\boldsymbol{J}_F\|_{L^2(F)} + \|J_F\|_{L^2(F)}\big). \tag{4.1}$$

The global error estimate and the maximal element error estimate over $\mathcal{T}_l$ are defined by

$$\eta_l := \Big(\sum_{K\in\mathcal{T}_l} \eta_K^2\Big)^{1/2}, \qquad \eta_{\max} = \max_{T\in\mathcal{T}_l} \eta_K.$$

4.1 Predicted error decrease strategy

The predicted error decrease strategy (PEDS) assumes that the solution is locally smooth and the optimal convergence can be obtained by either local h-refinement or local p-refinement. Then on each marked element K for refinement, an error decrease factor λ_K is computed to judge which of the h-refinement and p-refinement should be performed. We refer to [23, 26, 28] for various smooth-prediction strategies for the Poisson equation.

We shall extend the hp-adaptive algorithm of [26, Section 5.3.1] to Maxwell's equations. Assume that the solution $\boldsymbol{u}$ of (1.1) is smooth enough. Let $\hat{\mathcal{T}}_h$ be a tetrahedral mesh of Ω with $\max_{K\in\hat{\mathcal{T}}_h} = h$ and let $\hat{\boldsymbol{u}}_h \in \boldsymbol{U}(\hat{\mathcal{T}}_h, p)$ be the best approximation to $\boldsymbol{u}$ with respect to $\|\cdot\|_{\boldsymbol{H}(\mathbf{curl},\Omega)}$. Since $\big(V(\hat{\mathcal{T}}_h, p)\big)^3 \subset \boldsymbol{U}(\hat{\mathcal{T}}_h, p)$, we have

$$\begin{aligned}\|\boldsymbol{u} - \hat{\boldsymbol{u}}_h\|_{\boldsymbol{H}(\mathbf{curl},\Omega)} &= \inf_{\boldsymbol{v}_h\in\boldsymbol{U}(\hat{\mathcal{T}}_h,p)} \|\boldsymbol{u} - \boldsymbol{v}_h\|_{\boldsymbol{H}(\mathbf{curl},\Omega)} \le \inf_{\boldsymbol{v}_h\in(V(\hat{\mathcal{T}}_h,p))^3} \|\boldsymbol{u} - \boldsymbol{v}_h\|_{\boldsymbol{H}(\mathbf{curl},\Omega)} \\ &\le C h^{\min(p,m)} p^{-m} \|\boldsymbol{u}\|_{H^{m+1}(\Omega)} \qquad \forall m > 0. \end{aligned} \tag{4.2}$$

We are seeking for the discrete solution $\boldsymbol{u}_h \approx \hat{\boldsymbol{u}}_h$ by the hp-adaptive algorithm.

For any $K \in \mathcal{T}_l$, we let $T \in \mathcal{T}_{l-1}$ be its parent element satisfying $K \subseteq T$. If $K \in \mathcal{T}_{l-1} \cap \mathcal{T}_l$ is not refined in the $(l-1)$-level, we define $T := K$. We assume that $p_T = 2m$ holds locally

on T. Notice that the PEDS hp-adaptive algorithm starts from the uniform distribution of $p=1$. If $p_T<2m$, it will perform more p-refinements to achieve $p_T\approx 2m$. Then by (4.2), the local error decrease factors are heuristically defined by

$$\lambda_K=\left(\frac{p_T}{p_K}\right)^{p_T/2}\left(\frac{|K|}{|T|}\right)^{p_T/3}\approx\frac{\|\boldsymbol{u}-\boldsymbol{u}_l\|_{\boldsymbol{H}(\mathbf{curl},T)}}{\|\boldsymbol{u}-\boldsymbol{u}_{l-1}\|_{\boldsymbol{H}(\mathbf{curl},T)}}\qquad\forall K\in\mathcal{T}_l, \tag{4.3}$$

where $\boldsymbol{u}_l\in\boldsymbol{U}(\mathcal{T}_l,\mathcal{P}_l),\boldsymbol{u}_{l-1}\in\boldsymbol{U}(\mathcal{T}_{l-1},\mathcal{P}_{l-1})$ are the discrete solutions of (3.4). We refer to [26] for further discussions on the PEDS hp-adaptive algorithm for the Poisson equation. Using $\boldsymbol{u}_{l-1}$, we define the error indicator η_T on T as follows

$$\begin{aligned}\eta_T^2 &= h_T^2\Big(\Big\|\boldsymbol{f}+\kappa^2\alpha\boldsymbol{u}_{l-1}-\mathbf{curl}(\mu_r^{-1}\mathbf{curl}\,\boldsymbol{u}_{l-1})\Big\|^2_{L^2(T)}+\big\|\mathrm{div}(\boldsymbol{f}+\kappa^2\alpha\boldsymbol{u}_{l-1})\big\|^2_{L^2(T)}\Big) \\ &\quad+\frac{1}{2}\sum_{F\in\mathcal{F}(T)}h_F\Big(\Big\|[\mu_r^{-1}\mathbf{curl}\,\boldsymbol{u}_{l-1}\times\boldsymbol{n}]_F\Big\|^2_{L^2(F)}+\big\|[(\boldsymbol{f}+\kappa^2\alpha\boldsymbol{u}_{l-1})\cdot\boldsymbol{n}]_F\big\|^2_{L^2(F)}\Big).\end{aligned} \tag{4.4}$$

Algorithm 4.1 (PEDS)**.** Given a tolerance $\epsilon>0$ and the initial hp-pair $(\mathcal{T}_0,\mathcal{P}_0)$. Set $l=0$ and $\theta_1\in(0,1)$.

1. Solve the discrete problem (3.4) for $\boldsymbol{u}_{hp}\in\boldsymbol{U}(\mathcal{T}_l,\mathcal{P}_l)$. If $\alpha|_{\Omega_i}=0$, compute the $\boldsymbol{L}^2(\Omega)$-projection $\nabla\psi_{hp}\in\nabla V_c(\mathcal{T}_l,\mathcal{P}_l+1)$ of $\boldsymbol{u}_{hp}$ and set $\boldsymbol{u}_{hp}\leftarrow\boldsymbol{u}_{hp}-\nabla\psi_{hp}$.

2. Compute the local error estimators η_K for all $K\in\mathcal{T}_l$, the global error estimate η_l, and the maximal error estimate $\eta_{\max}$.

3. While $\eta_l>\epsilon$ do

   (a) Let $\hat{\mathcal{T}}_l=\{K\in\mathcal{T}_l:\eta_K>\theta_1\eta_{\max}\}$ be the set of elements marked for refinement.

   (b) Refine $\hat{\mathcal{T}}_l$ according to the predicted error decrease strategy:

   For any $K\in\hat{\mathcal{T}}_l$, compute λ_K by (4.3) *and η_T by* (4.4)*, do*
   $p_K\leftarrow p_K+1$, *if* $\eta_K\le\lambda_K\eta_T$,
   refining K using the bisection algorithm (see [25,30]), otherwise.
   Set $l\leftarrow l+1$.

   (c) Solve the discrete problem (3.4) for $\boldsymbol{u}_{hp}\in\boldsymbol{U}(\mathcal{T}_l,\mathcal{P}_l)$. If $\alpha|_{\Omega_i}=0$, set $\boldsymbol{u}_{hp}\leftarrow\boldsymbol{u}_{hp}-\nabla\psi_{hp}$ where $\nabla\psi_{hp}\in\nabla V_c(\mathcal{T}_l,\mathcal{P}_l+1)$ is the $\boldsymbol{L}^2(\Omega)$-projection of $\boldsymbol{u}_{hp}$.

   (d) Compute the local error estimators η_K for all $K\in\mathcal{T}_l$, the global error estimate η_l, and the maximal error estimate $\eta_{\max}$.

   end while.

4.2 The maximum strategy

We propose the the maximum strategy (MS) of the hp-adaptive algorithm. The heuristics behind the hp-adaptive algorithm is that

1. a subset of elements is marked for refinements on which the error is "large";

2. on each marked element K, if the solution is strongly singular (η_K is very large), do h-refinement; otherwise (weak singularity), do p-refinement.

Although the algorithm is simple, it shows good performances in our numerical experiments.

Algorithm 4.2 (MS)**.** Given a tolerance $\epsilon>0$ and the initial hp-pair $(\mathcal{T}_0,\mathcal{P}_0)$. Set $l=0$ and $0<\theta_1\leq\theta_2<1$. Replace Step 3 (b) in Algorithm 4.1 by Step (b)* :

(b)* Refine $\hat{\mathcal{T}}_l$ according to the maximum strategy:

$$\textit{Compute the average estimator}\quad \bar{\eta}=\Big(\sum\nolimits_{K\in\hat{\mathcal{T}}_l}\eta_K^2\Big)^{1/2}\Big(\sum\nolimits_{K\in\hat{\mathcal{T}}_l}1\Big)^{-1/2}.$$

$$\textit{For any}\quad K\in\hat{\mathcal{T}}_l,\quad \textit{do}$$

$$p_K\leftarrow p_K+1,\qquad \textit{if}\ \ \eta_K\leq\max\big\{\theta_2\eta_{\max},\theta_2^{-2}\bar{\eta}\big\},$$

$$\textit{bisection of } K,\qquad \textit{otherwise.}$$

$$\textit{Set } l\leftarrow l+1.$$

5 Numerical experiments

In the following, we report four numerical experiments to demonstrate the behavior of the hp-adaptive algorithms. Our implementation uses the hierarchical basis of the $\boldsymbol{H}(\mathbf{curl},\Omega)$-conforming edge element spaces [1] and the parallel adaptive finite element package PHG [39] which is based on unstructured meshes and MPI. We set the maximal polynomial degree as $\max\{p_K\in\mathcal{P}_l: l\geq 0\}=7$. The number of degrees of freedom (DOFs) is denoted by $N_{hp}=\dim\boldsymbol{U}(\mathcal{T}_h,\mathcal{P}_h)$.

In all numerical experiments, the experimental parameters are set by $\theta_1=\theta_2=0.7$ for the h-adaptive method, $\theta_1=0.3$ for the hp-adaptive method using Algorithm 4.1, and $\theta_1=0.3,\theta_2=0.7$ for the hp-adaptive method using Algorithm 4.2. In fact, setting

$$\theta_1=0.2,0.3\qquad\text{and}\qquad\theta_2=0.6,0.7,0.8$$

also yields exponential convergence of the hp-adaptive methods. But $(\theta_1,\theta_2)=(0.3,0.7)$ seems more efficient in our computations.

Example 5.1. The first example is the Fichera problem. We set $\Omega=(-1,1)^3\setminus[0,1]^3$ and $\mu_r=k=\alpha=1$ in (1.1). The righthand side $\boldsymbol{f}$ is so chosen that the exact solution of (1.1) is

$$\boldsymbol{u}(\boldsymbol{x})=\nabla\psi,\qquad \psi=\left(|\boldsymbol{x}|^2+\epsilon\right)^{1/4},\qquad \epsilon=10^{-6}.$$

Here ϵ is introduced to avoid accuracy loss of numerical integrations. In computations, we find that the accuracy of numerical integrations influences the optimality of the adaptive methods greatly.

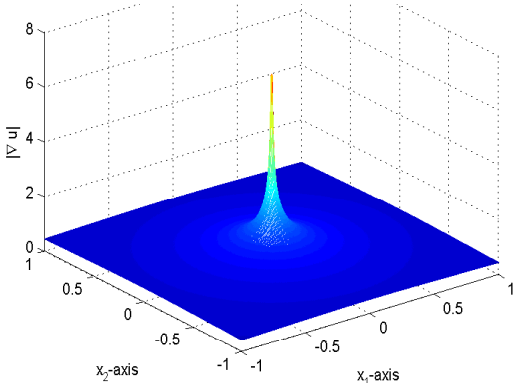

Figure 1: Graph of $|\boldsymbol{u}|$ on the slice $x_3=0$ (Example 5.1).

Figure 1 shows the graph of $|\boldsymbol{u}|$ in the x_1x_2-plane. Clearly the solution has strong singularity in the neighborhood of the origin. We use this experiment to demonstrate the efficiency of the hp-adaptive finite element methods for point singularities. The hp-adaptive iterations start from an initial mesh $\mathcal{T}_0$ with 336 elements and the polynomial degree distribution $\mathcal{P}_0=\{p_K=1:\forall K\in\mathcal{T}_0\}$.

Figure 2 shows the decreasing rates of the a posteriori error estimate and the approximation error. The curves are obtained by the h-adaptive method for $p=1$, the PEDS of the hp-adaptive method (Algorithm 4.1), and the MS of the hp-adaptive method (Algorithm 4.2). We find that the hp-adaptive methods performs much better than the h-adaptive method. Moreover, the exponential decay of both the a posteriori error estimate and the approximation error holds asymptotically

$$\eta_{hp}\approx Ce^{-\delta N_{hp}^{1/5}},\qquad \left\|\boldsymbol{u}-\boldsymbol{u}_{hp}\right\|_{\boldsymbol{H}(\mathbf{curl},\Omega)}\approx Ce^{-\delta N_{hp}^{1/5}},\qquad \delta=0.95.$$

Figure 3 shows two adaptively refined meshes using the PEDS algorithm and the MS algorithm. Figure 4 shows the polynomial degree distributions of the two meshes on the slice $\Sigma=\{\boldsymbol{x}\in\Omega:\,x_1=-0.001\}$. They display very fine meshes near the singularity. The right picture of Figure 4 shows that the MS algorithm uses lower-order polynomials near the singularity and high order polynomials elsewhere.

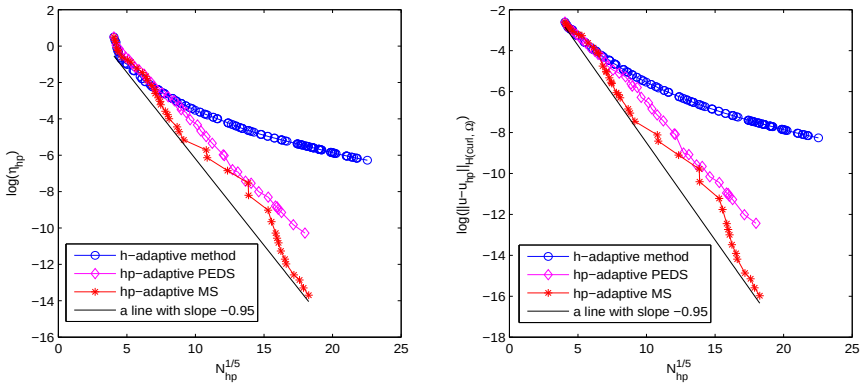

Figure 2: Convergence plots for the Fichera problem (Example 5.1).

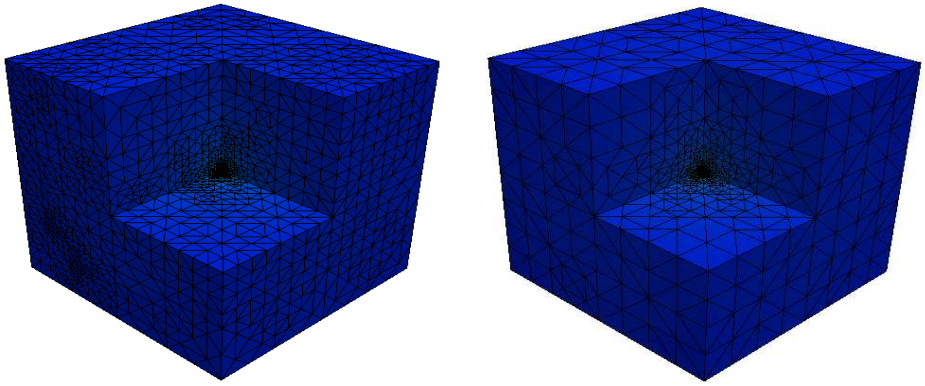

Figure 3: Adaptively refined meshes (Example 5.1). Left: 12169 elements by PEDS. Right: 9583 elements by MS.

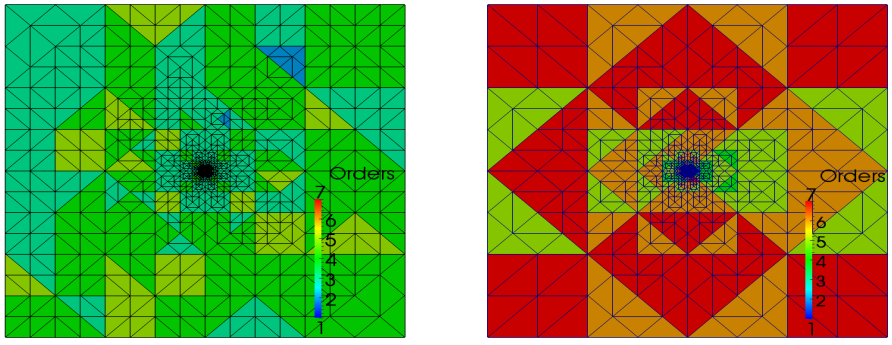

Figure 4: Polynomial degree distributions on the slice $x_1 = 0$ (Example 5.1). Left: PEDS. Right: MS

Example 5.2. Let $\Omega=(-1,1)^3\backslash\big([0,1]\times[0,1]\times[-1,1]\big)$ be an L-shaped domain and set $\mu_r=k=\alpha=1$ in (1.1). The righthand side $\boldsymbol{f}$ is so chosen that the exact solution of (1.1) is

$$\boldsymbol{u}(\boldsymbol{x})=\nabla\psi,\qquad \psi=\Big(\frac{r-x_1}{2}\Big)^{1/2},$$

where $r=\sqrt{x_1^2+x_2^2+\epsilon}$ and $\epsilon=10^{-6}$. Similarly the parameter ϵ is used to keep the accuracy of numerical integrations. Figure 5 and 6 show the graphs of $|\boldsymbol{u}|$ on the x_1x_2-plane, the x_2x_3-plane, and the x_1x_3-plane respectively. Clearly the solution $\boldsymbol{u}$ has an edge singularity along the x_3-axis.

We shall use this experiment to study the efficiency of the hp-adaptive finite element methods for single edge singularity. A shortcoming of shape-regular meshes is that it overrefines the mesh along singular edges so that the adaptive finite element method may not be optimal, especially for high-order finite elements. Therefore, anisotropic meshes are recommended near the edge singularities (cf. e.g. [6]). The optimality of the h-adaptive linear finite element method bas been demonstrated for edge singularities and the lowest order finite elements (see e.g. [16, 40]).

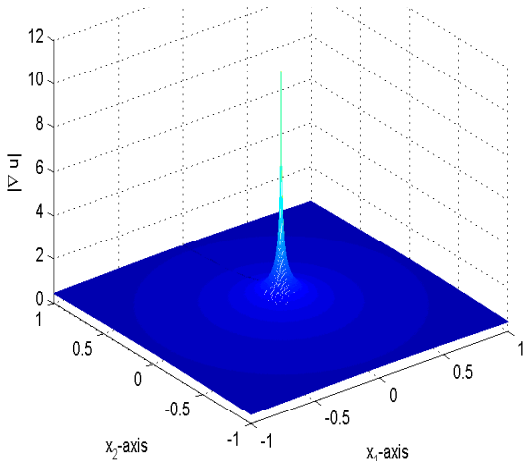

Figure 5: Graph of $|\boldsymbol{u}|$ on the slice $x_3=0$ (Example 5.2).

Since the hp-adaptive finite element method has varying polynomial degrees, the algebraic system from the discrete Maxwell's equations is difficult to solve. At present we use the parallel sparse direct solver MUMPS [33] to solve the algebraic system and can only deal with about 2 millions of unknowns. To study the efficiency of hp-adaptive methods for large-scale computations, we consider the discrete elliptic problem

$$\text{Find } \psi_h\in V(\mathcal{T}_h,\mathcal{P}_h):\qquad \int_\Omega\nabla\psi_h\cdot\nabla\varphi_h=-\int_\Omega\boldsymbol{f}\cdot\nabla\varphi_h\qquad\forall\,\varphi_h\in V(\mathcal{T}_h,\mathcal{P}_h).\tag{5.1}$$

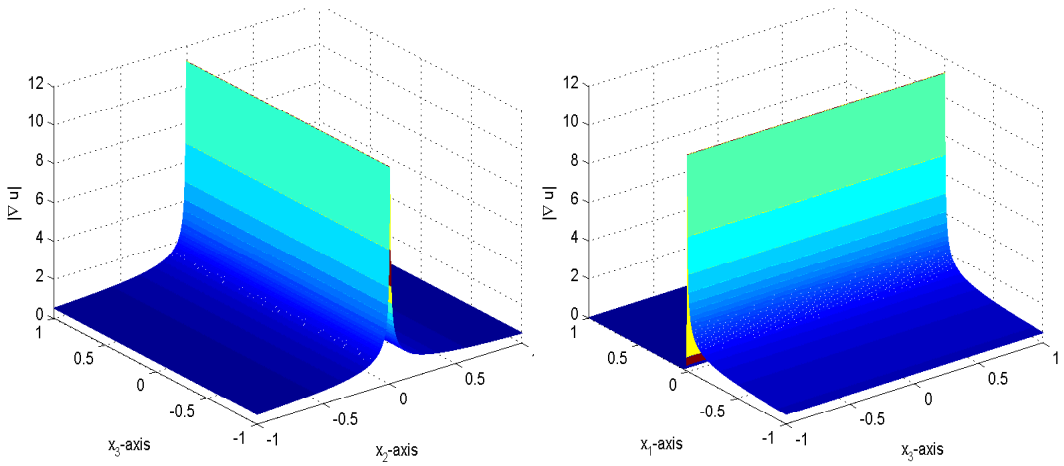

Figure 6: Graph of $|\boldsymbol{u}|$ on two slices. Left: $x_1=0$. Right: $x_2=0$ (Example 5.2).

It amounts to solve the discrete Maxwell equation (3.4) in a subspace $\nabla V(\mathcal{T}_h,\mathcal{P}_h)\subset \boldsymbol{U}(\mathcal{T}_h,\mathcal{P}_h)$. We use the following hp-type a posteriori error estimate for (5.1)

$$\eta_{hp}:=\Big(\sum_{K\in\mathcal{T}_h}\eta_K^2\Big)^{1/2},\qquad \eta_{\max}=\max_{T\in\mathcal{T}_h}\eta_K, \tag{5.2}$$

where the local error indicators are defined by

$$\eta_K=h_K\|\mathrm{div}(\boldsymbol{f}+\nabla\psi_h)\|_{L^2(K)}+\frac{1}{2}\sum_{F\in\mathcal{F}(K)}h_F^{1/2}\|[\boldsymbol{f}+\nabla\psi_h]_F\cdot\boldsymbol{n}\|_{L^2(F)}\qquad\forall K\in\mathcal{T}_h. \tag{5.3}$$

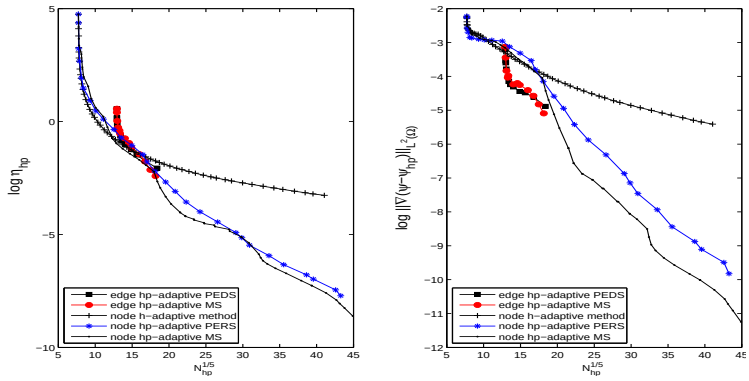

Figure 7: Convergence plots for the hp-adaptive finite element methods (Example 5.2).

Figure 7 shows the decreasing rates of the a posteriori error estimate η_{hp} and the approximation error $\|\nabla(\psi-\psi_h)\|_{\boldsymbol{L}^2(\Omega)}$. The curves are obtained by the h-adaptive nodal

element method with $p=1$ for solving (5.1), the PEDS of the hp-adaptive nodal element method for solving (5.1), and the MS of the hp-adaptive nodal element method for solving (5.1), the PEDS of the hp-adaptive edge element method for solving (3.4), and the MS of the hp-adaptive edge element method for solving (3.4). In our computations, the numbers of DOFs for the hp-adaptive methods are as follows

$$\begin{aligned} &\max N_{hp} = 1.83\times 10^8 && \text{for nodal elements,}\\ &\max N_{hp} = 2.03\times 10^6 && \text{for edge elements.} \end{aligned}$$

We find that the hp-adaptive methods perform much better than the h-adaptive method. Figure 8 shows two adaptively refined meshes obtained by the PEDS algorithm and the MS algorithm. Figure 9 shows the polynomial degree distributions on the slice $x_1=0$.

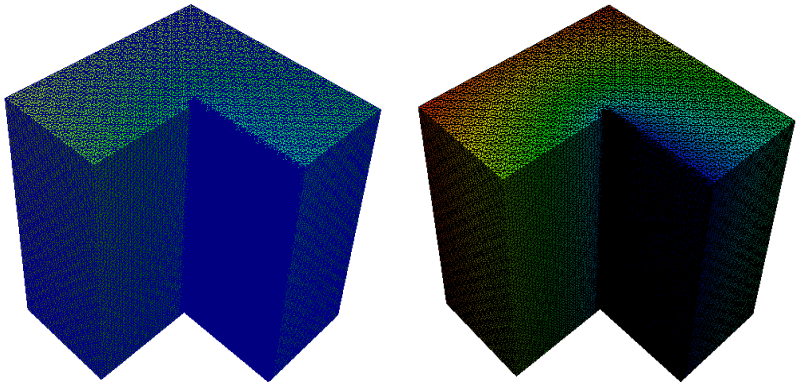

Figure 8: Adaptively refined meshes (Example 5.2). Left: 204288 elements by PEDS. Right: 208896 elements by MS.

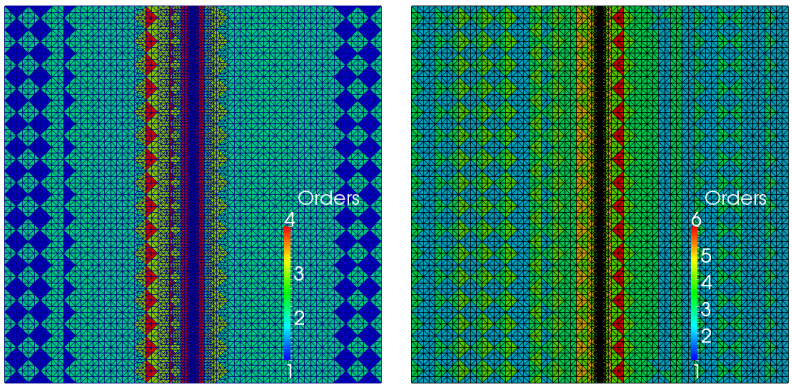

Figure 9: Polynomial degree distributions on the slice $x_1=0$ (Example 5.2). Left: PEDS. Right: MS

Example 5.3. The setting of this example is same to Example 5.2. To solve (5.1), we shall use a priori *hp*-adaptive finite element method based on anisotropic refinements along the edge of singularity. By comparing the numerical results with Example 5.2, we shall investigate the influence of the over-refinements on the efficiency of the isotropic *hp*-adaptive method.

First we partition Ω into cuboid meshes, and then subdivide each cuboid into six tetrahedrons [36]. We choose the nodes in both the x_1-direction and the x_2-direction as follows (see Figure 10)

$$0.0,\ \pm 0.2^J,\ \pm 0.2^{J-1},\ \cdots,\ \pm 0.2^2,\ \pm 0.2,\ \pm 1.0,$$

for some integer $J>0$. The nodes in the x_3-direction are chosen as

$$0.0,\ \pm 0.2,\ \pm 0.4,\ \pm 0.6,\ \pm 0.8,\ \pm 1.0.$$

The polynomial degrees are defined as follows

$$p_K = [1+j\cdot s] \qquad \forall K\in\mathcal{T}_h \text{ and } K\subset\Omega_j,\ 0\le j\le J, \tag{5.4}$$

where $[a]$ denotes the closest integer to a and

$$\Omega_0 := \left\{ \boldsymbol{x}\in\Omega : |x_1|\le 0.2^J, |x_2|\le 0.2^J \right\},$$
$$\Omega_j := \left\{ \boldsymbol{x}\in\Omega : 0.2^{J+1-j}\le |x_1|\le 0.2^{J-j}, 0.2^{J+1-j}\le |x_2|\le 0.2^{J-j} \right\}, \quad j=1,\cdots,J.$$

In our computations, we choose the parameters in (5.4) as $s=0.5,1.0$ and $J=1,2,\cdots,10$ respectively. We refer to [6] for more discussions on this anisotropic refinement strategy.

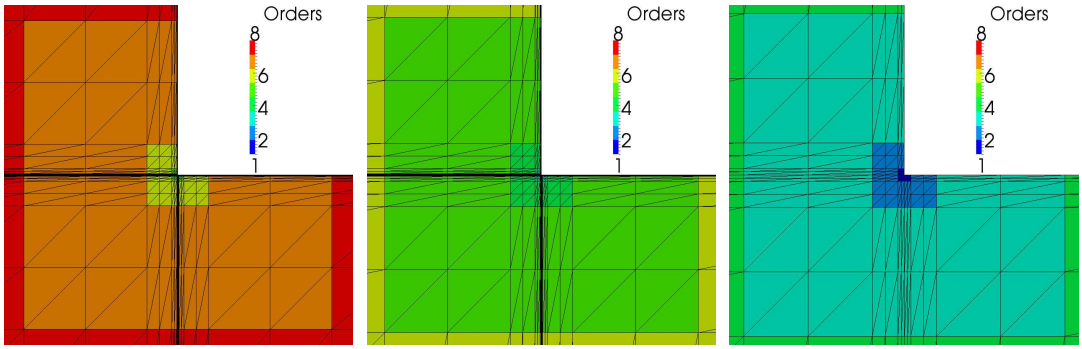

Figure 10: An anisotropic mesh and the distribution of polynomial degrees on the slice $x_3=0$. From left to right: the figures are zoomed in successively near the singularity (Example 5.3).

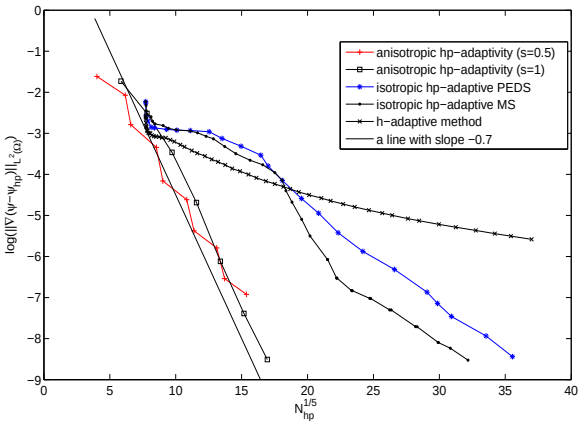

Figure 11: Decrease rates of the error produced by the anisotropic hp-adaptive method, the isotropic hp-adaptive methods, and the h-adaptive method (Example 5.3).

Figure 10 shows an anisotropic mesh and the distribution of polynomial degrees over this mesh. Figure 11 shows the decrease rates of the error obtained by the anisotropic hp-adaptive method, the isotropic hp-adaptive method, and the h-adaptive method. For the case that $s=1$ in (5.4), we find that the anisotropic hp-adaptive method leads to exponential decay of the error

$$\|\nabla(\psi-\psi_{hp})\|_{L^2(\Omega)} \approx Ce^{-\delta N_{hp}^{1/5}}, \qquad \delta = 0.7.$$

We also find that the isotropic hp-adaptive method is less efficient than the anisotropic hp-adaptive method but still more efficient than the h-adaptive method.

Example 5.4. Set $\Omega=(-1,1)^3\backslash[0,1]^3$ and $\mu_r=k=\alpha=1$ in (1.1). The righthand side $\boldsymbol{f}$ is so chosen that the exact solution of (1.1) is

$$\boldsymbol{u}(\boldsymbol{x})=\nabla\psi, \qquad \psi=\sum_{i=1}^{3}\left(\frac{r_i-x_i}{2}\right)^{1/2}, \qquad r_i=\left(x_i^2+x_{i+1}^2+\epsilon\right)^{1/2},$$

where $x_4:=x_1$ and $\epsilon=10^{-6}$. Figure 12 shows the graph of $|\boldsymbol{u}|$ in the x_1x_2-plane. The solution $\boldsymbol{u}$ has singularities along three axes. We shall use this experiment to demonstrate the efficiency of the hp-adaptive methods for multiple edge singularities.

We still solve the discrete Maxwell's equations (3.4) and the elliptic problem (5.1) by hp-adaptive finite element methods. The a posteriori error estimate for (5.1) is defined in (5.2) and (5.3). Figure 13 shows the decreasing rates of the a posteriori error estimate η_{hp} and the approximation error $\|\nabla(\psi-\psi_h)\|_{L^2(\Omega)}$. The curves are obtained by the h-adaptive nodal element method for $p=1$, the PEDS of the hp-adaptive nodal element method, and the MS of the hp-adaptive nodal element method, the PEDS of the

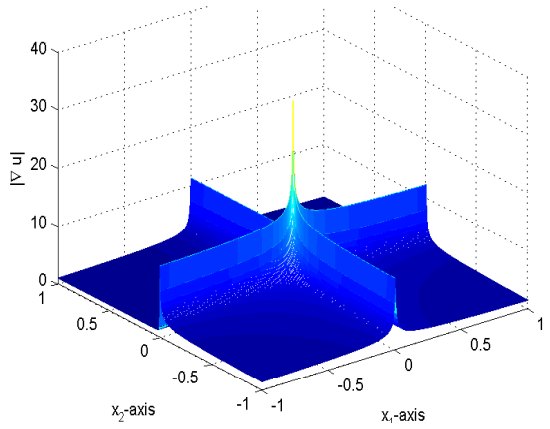

Figure 12: Graph of $|\boldsymbol{u}|$ on the slice $x_3 = 0$ (Example 5.4).

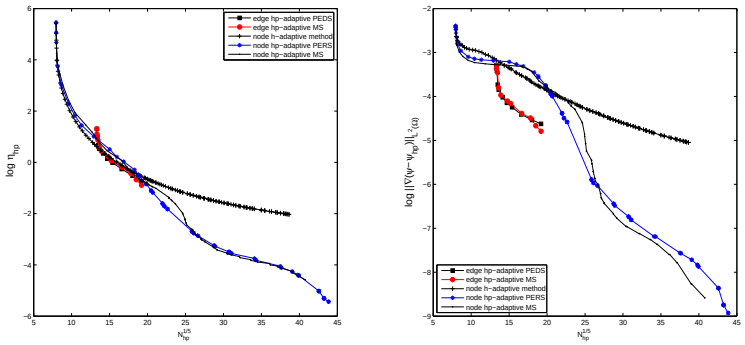

Figure 13: Convergence plots for the hp-adaptive finite element methods (Example 5.4).

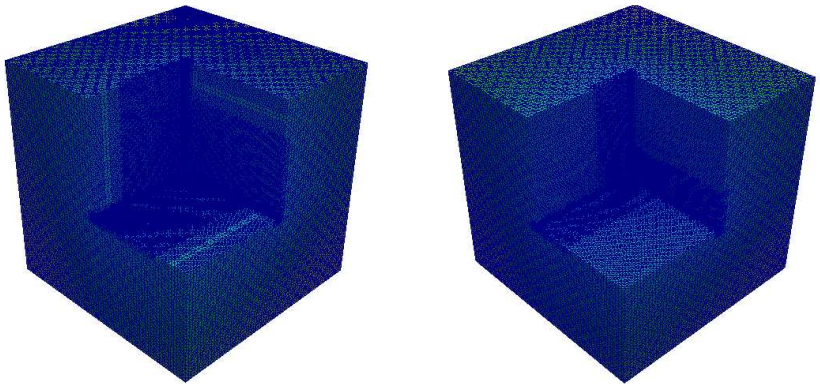

Figure 14: Adaptively refined meshes (Example 5.4). Left: 234029 elements by PEDS. Right: 220883 elements by MS.

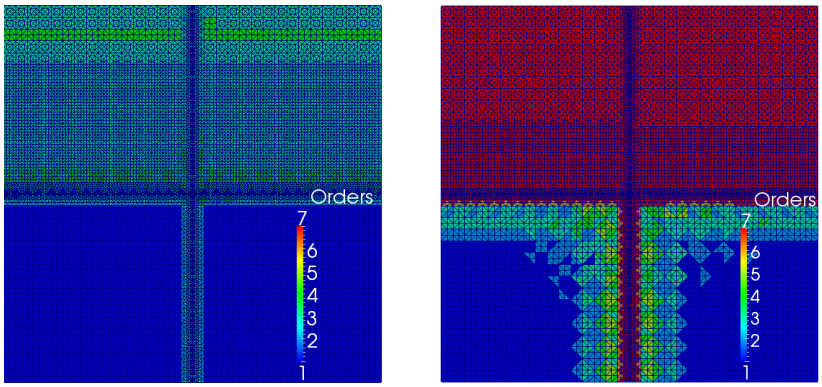

Figure 15: Polynomial degree distributions on the slice $x_1 = 0$ (Example 5.4). Left: PEDS. Right: MS

hp-adaptive edge element method, and the MS of the hp-adaptive edge element method. In our computations, the numbers of DOFs for the hp-adaptive methods are as follows

$$\begin{aligned} \max N_{hp} &= 1.62 \times 10^8 \qquad \text{for nodal elements,} \\ \max N_{hp} &= 2.62 \times 10^6 \qquad \text{for edge elements.} \end{aligned}$$

From Figure 13, we still find that the hp-adaptive methods performs much better than the h-adaptive method. Figure 14 shows two adaptively refined meshes obtained by the PEDS algorithm and the MS algorithm. Figure 15 shows the polynomial degree distributions on the slice $x_1 = 0$. Near the singular edges, the hp-adaptive methods generate very fine mesh and use lower-order polynomials, while it uses higher order polynomials away from the edge singularities.

Example 5.5. The fourth example is Team Benchmark Problem 21-a2 (see [18]). This problem consists of a non-magnetic steel plate with two slits and two racetrack shaped coils (see Figure 16). The steel plate has a conductivity of 1.3889×10^6 Siemens/Metre. The sinal driving current for each coil is 3000 Ampere/Turn and has a frequency of 50 Hz. The driving currents for the two coils are in opposite directions. We solve the discrete Maxwell's equations (3.4) by hp-adaptive finite element methods.

Figure 17 shows the decreasing rates of the a posteriori error estimate by the h-adaptive method for $p = 1$, the PEDS of the hp-adaptive method, and the MS of the hp-adaptive method. We find that the hp-adaptive methods show great superiority over the h-adaptive method in reducing the error. Again we find that the exponential decay of the a posteriori error estimate holds asymptotically :

$$\eta_{hp} \approx C e^{-\delta N_{hp}^{1/5}}, \qquad \delta = 0.3.$$

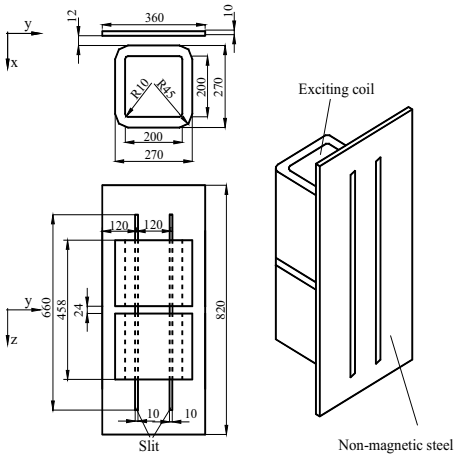

Figure 16: The geometry of Team Workshop Problem 21-a2 (Example 5.2).

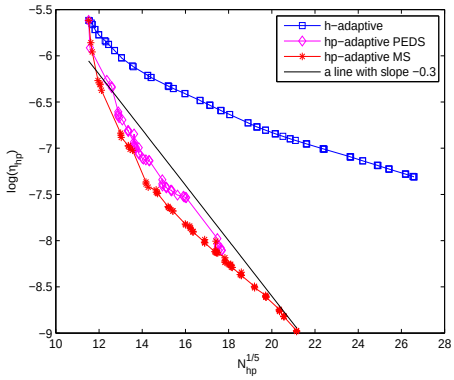

Figure 17: Convergence plots for the eddy current problem (Example 5.5).

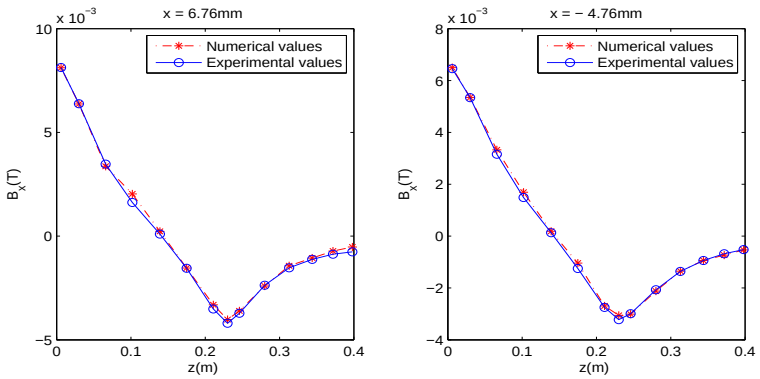

Figure 18: Values of B_1 on two lines inside Ω (MS).

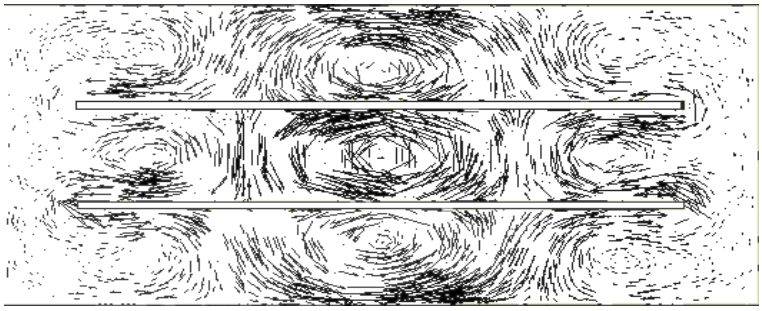

Figure 19: Eddy current distribution on a slice of the steel plate (MS).

Figure 18 shows the values of the first component of the magnetic flux $\boldsymbol{B}$ along two lines

$$\{\boldsymbol{x}: x_1 = 0.00676, x_2 = 0.0\} \qquad \text{and} \qquad \{\boldsymbol{x}: x_1 = -0.00476, x_2 = 0.0\}$$

which correspond to the two lines $\{\boldsymbol{x}: x_1 = \pm 0.00576, x_2 = 0.0\}$ in [18] respectively. Figure 19 shows the eddy current distribution on a slice of the steel plate. The numerical data are computed by Algorithm 4.2 and coincide very well with the experimental values.

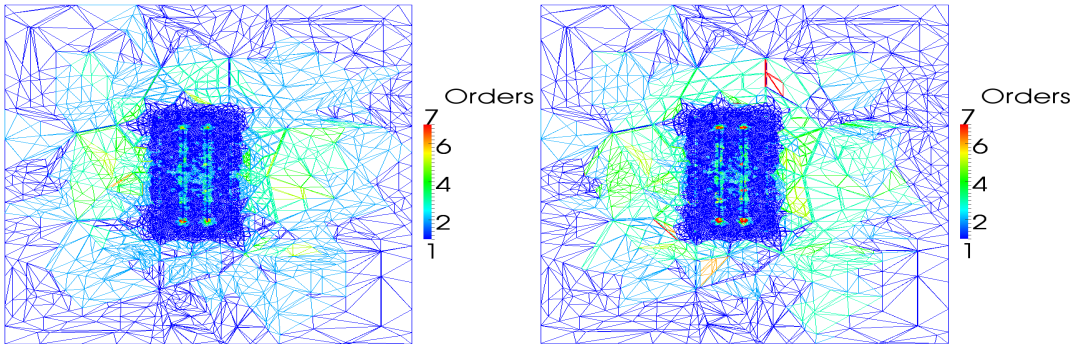

Figure 20: Polynomial degree distribution on the slice $x_1 = 0.005999$. Left: $(\mathcal{T}_{48}, \mathcal{P}_{48})$ by the PEDS algorithm. Right: $(\mathcal{T}_{47}, \mathcal{P}_{47})$ by the MS algorithm. (Example 5.2)

Figure 20 shows the hp-pairs $(\mathcal{T}_{48}, \mathcal{P}_{48})$ by Algorithm 4.1 and $(\mathcal{T}_{47}, \mathcal{P}_{47})$ by Algorithm 4.2 on the slice $\Sigma_1 = \{\boldsymbol{x} \in \Omega : x_1 = 0.005999\}$, where

$$\begin{aligned} \dim \boldsymbol{U}(\mathcal{T}_{48}, \mathcal{P}_{48}) &= 1801958 \quad \text{for Algorithm 4.1,} \\ \dim \boldsymbol{U}(\mathcal{T}_{47}, \mathcal{P}_{47}) &= 1729148 \quad \text{for Algorithm 4.2.} \end{aligned}$$

The two algorithms yield very similar distributions of elements and polynomial degrees. From the figures, we find roughly that the hp-adaptive methods use

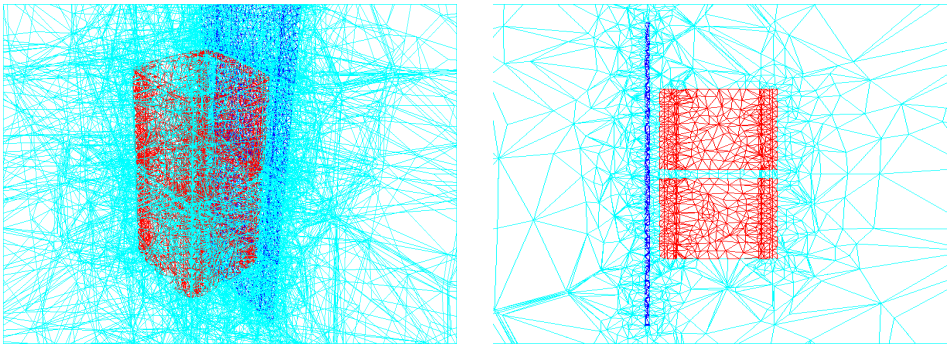

Figure 21: An adaptively refined mesh after 47 hp-adaptive iterations from the initial mesh (Example 5.2).

1. lower order elements near the boundary where the error is very small,

2. lower order elements in the conducting domain where the solution varies rapidly,

3. and high order elements in the insulating region away from the boundary where the error is moderate.

Since the solution varies rapidly in the conducting domain, $\mathcal{T}_{47}$ displays a fine mesh there in Figure 21.

Acknowledgments

The authors are grateful to Dr. Hui Liu and Dr. Tao Cui from Chinese Academy of Sciences for their inspiring discussions on the hp-adaptive algorithms. The work of Linbo Zhang was supported in part by the National Basic Research Project under the grant 2011CB309703, by the Funds for Creative Research Groups of China (Grant No. 11021101), and by China NSF under the grant 60873177. The work of Weiying Zheng was supported in part by China NSF under the grants 11031006 and 11171334, by the Funds for Creative Research Groups of China (Grant No. 11021101), and by the National Magnetic Confinement Fusion Science Program (Grant No. 2011GB105003).

References

[1] M. Ainsworth and J. Coyle, Hierarchic finite element bases on unstructured tetrahedral meshes, Int. J. Numr. Meth. Engng., 58 (2003), 2103–2130.
[2] M. Ainsworth and B. Senior, An adaptive refinement strategy for hp-finite element computation, Appl. Numer. Math., 26 (1998), 165–178.
[3] H. Ammari, A. Buffa, and J.C. Nédélec, A justification of eddy current model for the maxwell equations, SIAM J. Appl. Math., 60 (2000), 1805-1823.

[4] D.N. Arnold, A. Mukherjee, and L. Pouly, Locally Adapted Tetrahedral Meshes Using Bisection, SIAM J. Sci. Comput., 22 (2000), 431-448.
[5] I. Babuška and A. Aziz, Survey Lectures on Mathematical Foundations of the Finite Element Method, in The Mathematical Foundations of the Finite Element Method with Application to the Partial Differential Equations, ed. by A. Aziz, Academic Press, New York, 1973.
[6] I. Babuška, B. Andersson, B. Guo, J.M. Melenk, and H.S. Oh, Finite element method for solving problems with singular solutions, J. Comput. Appl. Math., 74 (1996), 51-70.
[7] I. Babuška and M.R. Dorr, Error estimates for combined h and p versions of the finite element method, Numer. Math., 37 (1981), 257-277.
[8] I. Babuška and C. Rheinboldt, Error estimates for adaptive finite element computations, SIAM J. Numer. Anal., 15 (1978), 736-754.
[9] I. Babuška, B.A. Szabo, and I.N. Katz, The p-version of the finite element method, SIAM J. Numer. Anal., 18 (1981), 515-545.
[10] F. Bachinger, U. Langer, and J. Schöberl, Numerical analysis of nonlinear multiharmonic eddy current problems, Numer. Math., 100 (2005), pp. 594-616.
[11] R. Beck, R. Hiptmar, R.H.W. Hoppe, and B. Wohlmoth, Residual based a posteriori error estimations for eddy current computation, M2AN Math. Modeling and Numer. Anal., 34 (2000), 159-182.
[12] M.Sh. Birman and M.Z. Solomyak, L^2-Theory of the Maxwell operator in arbitary domains, Uspekhi Mat. Nauk 42 (1987), pp. 61-76 (in Russian); Russian Math. Surveys 43 (1987), pp. 75-96 (in English).
[13] D. Braess, V. Pillwein, and J. Schöberl, Equilibrated residual error estimators are p-robust, Comput. Methods Appl. Mech. Eng., 198 (2009), 1189-1197.
[14] D. Braess and J. Schöberl, Equilibrated residual error estimator for edge elements, Math. Comp., 77 (2008), 651-672.
[15] J. Chen, Z. Chen, T. Cui and L. Zhang, An adaptive finite element method for the eddy current model with circuit/field couplings, SIAM J. Sci. Comput., 32 (2010), 1020-1042.
[16] Z. Chen, L. Wang, and W. Zheng, An adaptive multilevel method for time-harmonic Maxwell equations with singularities, SIAM J. Sci. Comput., 29 (2007), 118-138.
[17] Z. Chen, B. Guo, and Y. Xiao, An hp adaptive uniaxial perfectly matched layer method for Helmholtz scattering problems, Commun. in Comput. Phys., 5 (2009), 546-564.
[18] Z. Cheng, N. Takahashi, and B. Forghani, TEAM Problem 21 Family (V. 2009), approved by the International Compumag Society Board at Compumag-2009, Florianópolis, Brazil, http://www.compumag.org/jsite/team.html .
[19] L. Demkowicz, J. Kurtz, D. Pardo, M. Paszyński, W. Rachowicz, and A. Zdunek, Computing with hp-Adaptive Finite Elements, Vol. 2, Frontiers: Three Dimensional Elliptic and Maxwell Problems with Applications, Chapman & Hall/CRC, Boca Raton, London, 2008.
[20] A.B. Dhia, C. Hazard, and S. Lohrengel, A singular field method for the solution of Maxwell's equations in polyhedral domains, SIAM J. Appl. Math., 59 (1999), pp. 2028-2044.
[21] W. Dörfler, A convergent adaptive algorithm for Poissons equation, SIAM J. Numer. Anal., 33 (1996), 1106-1124.
[22] W. Guo and I. Babŭska, The h-p version of the finite element method. Part 2. General results and applications, Comput. Mech., 1 (1986), 203–226.
[23] V. Heuveline and R. Rannacher, Duality-based adaptivity in the hp-finite element method, J. Numer. Math., 11 (2003), 1–18.
[24] R. Hoppe and J. Schöberl, Convergence of adaptive edge element methods for the 3D eddy currents equation, J. Comp. Math., 27 (2009), 657-676.

[25] I. Kossaczký, A recursive approach to local mesh refinement in two and three dimensions, J. Comput. Appl. Math., 55 (1994), 275–288.
[26] H. Liu, Researches on Dynamic Load Balancing Algorithms and hp Adaptivity in 3-D Parallel Adaptive Finite Element Computations, Ph.D thesis, Academy of Mathematics and Systems Science, Chinese Academy of Sciences, 2010 (accessible by sending email to Dr. Liu Hui : liuhui@lsec.cc.ac.cn).
[27] J.M. Melenk, hp-interpolation of nonsmooth functions and an application to hp-a posteriori error estimation, SIAM J. Numer. Anal., 43 (2005), 127–155.
[28] J.M. Melenk and B. Wohlmuth, On residual-based a posteriori error estimation in hp-FEM, Adv. Comp. Math., 15 (2001), 311–331.
[29] W.F. Mitchell and M.A. McClain, A survey of hp-adaptive strategies for elliptic partial differential equations, Recent Advances in Computational and Applied Mathematics, T.E. Simos (Ed.), Springer Dordrecht, 2011.
[30] W. MITCHELL, *Optimal multilevel iterative methods for adaptive grids*, SIAM J. Sci. Stat. Comput., 13 (1992), pp. 146–167.
[31] P. Monk, Finite Element Methods for Maxwell's Equations, Clarendon Press, Oxford, 2003.
[32] P. Morin, R.H. Nochetto, and K. Siebert, Convergence of adaptive finite element methods, SIAM Review, 44 (2002), 631-658.
[33] MUMPS: a MUltifrontal Massively Parallel sparse direct Solver. http://mumps.enseeiht.fr .
[34] D. Pardo, L. Demkowicz, C. Torres-Verdín, and M. Paszynski, Two-dimensional high-accuracy simulation of resistivity logging-while-drilling (lwd) measurements using a self-adaptive goal-oriented hp finite element method, SIAM J. Appl. Math., 66 (2006), 2085-2106.
[35] D. Pardo, L. Demkowicz, C. Torres-Verdín, and M. Paszynski, A self-adaptive goal-oriented hp-finite element method with electromagnetic applications. Part II: Electrodynamics, Computer Methods in Applied Mechanics and Engineering, 196 (2007), 37-40.
[36] A. Schmidt and K.G. Siebert, Design of Adaptive Finite Element Software, The Finite Element Toolbox ALBERTA, Lecture Notes in Computational Science and Engineering, Vol. 42, Springer, Berlin, 2005.
[37] J. Schöberl, A posteriori error estimates for Maxwell equations, Math. Comp., 77 (2008), 633-649.
[38] R. Verfürth, A Review of A Posteriori Error Estimation and Adaptive Mesh-Refinement Rechniques, Wiley-Teubner, Chichester, Stuttgart, 1996.
[39] L. Zhang, A Parallel Algorithm for Adaptive Local Refinement of Tetrahedral Meshes Using Bisection, Numer. Math.: Theor. Method Appl., 2 (2009), 65-89.
[40] W. Zheng, Z. Chen, and L. Wang, An adaptive finite element method for the $\boldsymbol{H}$–ψ formulation of time-dependent eddy current problems, Numer. Math., 103 (2006), 667-689.